Chinese Chemical Letters 31 (2020) 2730–2736

Contents lists available at ScienceDirect

Chinese Chemical Letters

journal homepage: www.elsevier.com/locate/cclet

Communication

Degradation of tartrazine by peroxymonosulfate through magnetic Fe_2O_3/Mn_2O_3 composites activation

Gong Chen[a], Li-Chao Nengzi[b], Yingjie Gao[a], Guixian Zhu[a], Jianfeng Gou[a], Xiuwen Cheng[a,b,*]

[a] Key Laboratory of Western China's Environmental Systems (Ministry of Education) and Key Laboratory for Environmental Pollution Prediction and Control, Gansu Province, College of Earth and Environmental Sciences, Lanzhou University, Lanzhou 730000, China
[b] Academy of Economics and Environmental Sciences, Xichang University, Xichang 615000, China

ARTICLE INFO

Article history:
Received 4 January 2020
Received in revised form 9 February 2020
Accepted 17 February 2020
Available online 18 February 2020

Keywords:
Fe_2O_3/Mn_2O_3
Peroxymonosulfate
Tartrazine
Degradation
Activation
Mechanism

ABSTRACT

In this study, Fe_2O_3/Mn_2O_3 composite was synthesized by a facile two-step technique, and several methods were carried out to characterize it. Then, the decomposition experiments of tartrazine (TTZ), a kind of refractory organic pollutant, were conducted under various environmental condition to detect the catalyst performance, such as reaction system, the dosage of catalyst, peroxymonosulfate (PMS) concentration, initial pH, different natural water substances. The results exhibited that Fe_2O_3/Mn_2O_3 composite with the mole rate 2:3 had the best PMS activation performance and the removal efficiency was 97.3% within 30 min. Besides, the optimum degradation conditions of TTZ were also discussed, that is catalyst dosage (0.6 g/L), PMS concentration (0.8 g/L) and the initial pH 11. In addition, proved by the natural water substances adding experiments, HPO_4^{2-}, HCO_3^-, NO_3^- and NOM (nature organic matter) could slow down the experiments progressing, but Cl^- could boost it. Then inhibitor experiments indicated both the $HO^•$ and $SO4^{•-}$ played a vital role in the experiments. Reusability and ions leaching experiments as well as the used catalyst physical characterization images exhibited the excellent stability and cyclicity of the Fe_2O_3/Mn_2O_3 composite. Finally, based on the XPS (X-ray photoelectron spectroscopy) and the experiments results, the possible mechanism of TTZ degradation was proposed. This system might provide a novel thought for the decomposition of refractory organic pollutant and had potential in promotion of actual sewage treatment technology.

Because of uniform color, high tolerance to oxidation and heating conditions, tartrazine (TTZ) is widely used in the food additive and colorant [1,2]. However, with heavy use in industry and life, the danger of the TTZ gradually emerges. Previous studies had shown that TTZ possibly gave rise to adverse physique influences such as chronic poisoning, hindering children's intellectual development, asthma and carcinogenicity [3]. But as a result of its stability, existing sewage treatment methods cannot completely remove it, and TTZ could accumulate in the environment and might cause greater potential threats [4]. At present, it is imperative to put forward a fast and effective method for TTZ removal. Hasna *et al.* used zinc-aluminum layered double hydroxide to adsorb TTZ dye from aqueous solution and the removal efficiency reached 98.9% within 60 min. Also, electro-Fenton reactor was utilized to TTZ degradation by Zhang *et al.* with the TTZ removal of 80% after 12 h continuous operations. Marija *et al.* synthesized Co(II) impregnated Al(III)-pillared montmorillonite to activate peroxymonosulfate (PMS) to degrade TTZ and the decolorization was 93.5% within 120 min [5–7]. These studies have great significance to disposal of TTZ, but the material repeatability, TTZ degradation speed and efficiency limited their application. This study is to find a better method to degrade TTZ.

Owing to the production of reactive oxygen species (ROS, such as hydroxyl radical $HO^•$ and sulfate radical $SO4^{•-}$), advanced oxidation processes (AOPs) can oxidize or degrade refractory macromolecules to reduce their harm [8]. $HO^•$ and $SO4^{•-}$ possess higher redox potential (2.8 V and 2.5–3.1 V, respectively), which can contribute to destroy the structure of macromolecules [9–12]. The AOPs have the advantages of rapid reaction, easy application and high activity, so they were gradually taken seriously by people. Ordinarily, people activate PMS by ultrasound, ultraviolet,

* Corresponding author at: Key Laboratory of Western China's Environmental Systems (Ministry of Education) and Key Laboratory for Environmental Pollution Prediction and Control, Gansu Province, College of Earth and Environmental Sciences, Lanzhou University, Lanzhou 730000, China.
E-mail address: chengxw@lzu.edu.cn (X. Cheng).

transition elements, metallic oxide, and thermal energy to produce ROS [13]. However, for economy and convenient operation, the transition elements and metallic oxide look like an optimal PMS activation mode.

Through the above discussion, to propose a catalyst which can activate PMS to generate the ROS for efficient contaminants elimination is meaningful and vital for the application of AOPs in actual water disposal. As a heterogeneous catalyst, compared with homogeneous catalyst, metal oxide is easier to recycle and causes less environmental pollution, it attracts more attention. Owing to the rich reserves, inexpensive and environment friendly characteristics, Fe and Mn oxides are considered as preferred activators for PMS. Huang *et al.* utilized MnO_2 with different structures to activate PMS to degrade Bisphenol A, and the best removal efficiency was 94.5% within 10 min [10]. Ramin *et al.* obtained 88.5% degradation rate of cyfluthrin through PMS activated by Fe_2O_3/AC mesoporous heterojunction within 80 min [14]. Ma *et al.* utilized Fe_2O_3/Mn_3O_4 to activate PS (persulfate) for rhodamine B (Rh B) decomposition and achieved good success [15]. These researches, to some extent, prove the feasibility of PMS activation by Fe and Mn oxides to remove organic pollutant. In this work, we synthesized a novel magnetic Fe_2O_3/Mn_2O_3 composite by a handy method as an activator of PMS. Compared with the above catalysts, this as-prepared catalyst possesses magnetism in order to facilitate recycling and its preparation method is simple. Moreover, we take advantage of Fe_2O_3/Mn_2O_3@PMS system to degrade refractory organic TTZ under different conditions to detect its efficiency.

In this study, the magnetic Fe_2O_3/Mn_2O_3 composites were synthesized through a handy way and the main materials and agentia used were exhibited in Supporting information. Specifically, an appropriate mole proportion of $MnSO_4{\cdot}H_2O$ and $K_3[Fe(CN)_6]$ (with Mn/Fe of 1:1, 3:2 and 2:3) were dissolved in three beakers respectively, stirring to dissolve completely. The mixed suspension was aged at room temperature for 24 h without any interruption, after that, centrifuged and the lower layer precipitate was washed with water and ethanol for 3 times respectively. Then the sediment was put into an oven to dry at 60 °C for 8 h. Finally, the dried precipitate was calcined at 450 °C for 2 h with the heating rate of 2 °C/min in the air (**CAUTION: Be careful not to burn yourself**). Cool to room temperature naturally and the required magnetic Fe_2O_3/Mn_2O_3 composites were obtained.

After the synthesis, the morphology and elemental analysis of Fe_2O_3/Mn_2O_3 composites catalysts were detected by SEM (scanning electron microscope), EDS (energy dispersive spectrometer) and Mapping (Japan Electron Optics Laboratory Co., Ltd. JSM-6701 F). XRD (X-ray diffraction) atlas of the catalysts was achieved on a D/Max-2004 X-ray powder diffractometer (Bruker, Germany) with Cu Kα radiation (λ = 0.15425 nm). Moreover, XPS (X-ray photoelectron spectroscopy) (Kratos AXIS Ultra DLD) spectrum was done with an Al Kα (1486.6 eV) source for getting a better understanding of the role of Mn, Fe, and O species in the Fe_2O_3/Mn_2O_3@PMS system.

Next, we conducted a serious of degradation experiments and the experimental design was as follows. Based on the actual situation, 10 mg/L TTZ was selected as the target contaminant concentration in the work. Put 50 mL of TTZ solution into 150 mL conical flasks and put them in a wobbly machine in which set the oscillation frequency and reaction temperature were 180 rpm and 25 °C, respectively. During each experiment, a set number of Fe_2O_3/Mn_2O_3 and PMS were added in flasks according to the experimental design. Then, at certain time intermission, 3 mL of the solution was taken from the flasks with a disposable syringe and extracted with a 0.22 μm filter membrane. Immediately the absorbance of the extracting solution was measured by T6 UV–vis spectrophotometer (Persee, Beijing) at the utmost absorption wavelengths of the TTZ (427 nm). Moreover, some pivotal factors that could affect TTZ degradation were detected too. We also degrade some common contaminants (such as Rh B, malachite green (MG), amino black (AB), methyl orange (MO) and methylene blue (MB)) to test the practical applicability of the Fe_2O_3/Mn_2O_3@PMS system in this work.

XRD patterns of the Fe_2O_3/Mn_2O_3 were displayed in Fig. 1a. As clearly shown, they were all perfectly matched with the standard based on their JCPDS cards. At the XRD pattern of Fe_2O_3/Mn_2O_3, a sharp peak (2θ = 35.64°) was related to (104) plane of Fe_2O_3 (JCPDS No. 73-0603) and other seven intense peaks at 2θ = 30.0°, 32.9°, 42.9°, 53.3°, 57.0°, 60.6° and 62.3° could be indexed to (310), (222), (420), (521), (035), (611) and (026) crystal plane of Mn_2O_3 (JCPDS No. 76-0150) respectively. In addition, comparing fresh and used XRD pattern of Fe_2O_3/Mn_2O_3 (Mn/Fe = 3:2), we could see that although the intensity of some peaks decreased slightly after the reaction, their positions remained basically unchanged and no new peaks appeared. To a certain extent, this result proved that the Fe_2O_3/Mn_2O_3 composites had been successfully fabricated and possessed outstanding stability.

XPS measurements were conducted to characterize elemental component and oxidation state of Fe_2O_3/Mn_2O_3 composite and the corresponding results were exhibited in Fig. 1b. As shown at Fig. 1b, C 1s, O 1s, Mn 2p and Fe 2p peaks appeared in the XPS full-scale spectrum evidently which demonstrated presence of these elements in the as-prepared samples [16,17]. Both in the fresh and used samples, three peaks were exhibited at Mn 2p high resolution scan (Fig. 1c), and the position of the peaks had no obvious shift. In addition, based on previous researches, the peaks at 644.4 eV and 642.1 eV corresponded to Mn(IV) and Mn(III) [18,19]. Moreover, it could be clearly seen in Fig. 1c that approximately 5% Mn(III) converted to Mn(IV) after cyclic reaction. Which was ascribed to the mutual transformation of Mn(III)/Mn(IV) during activating PMS. The Fig. 1d exhibited the condition of Fe element in the degradation experiments. As shown, there were two obvious peaks in the fresh sample and after experiments an extra peak emerged. According to the predecessors' literatures, Fe(III) would convert to Fe(II) in the activation of PMS which coincided with the above phenomena [20]. These results would be

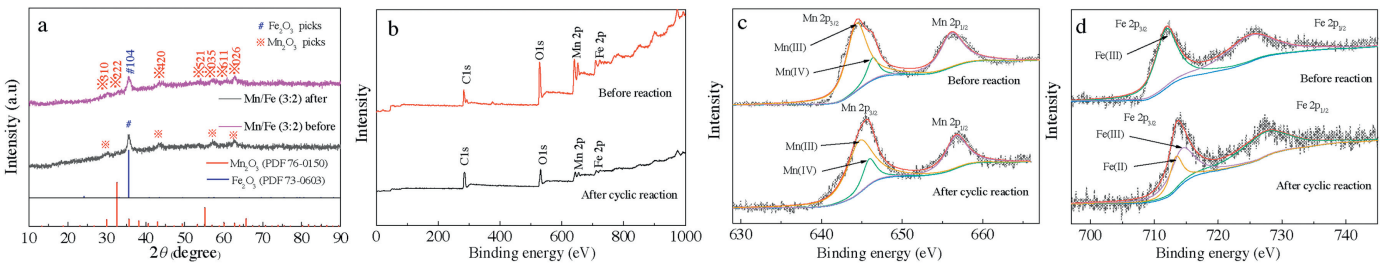

Fig. 1. XRD patterns of Fe_2O_3/Mn_2O_3 composite (a), XPS survey spectra of Fe_2O_3/Mn_2O_3 composite (b) and corresponding Mn 2p (c) and Fe 2p peak (d) of the composites (before and after cyclic reaction).

of great significance in the subsequent analysis of reaction mechanism.

The SEM and Mapping technique were hired to measure the morphology and element distribution of the Fe_2O_3/Mn_2O_3 composite (Fig. 2a). The SEM images revealed that this catalyst consists of two substances with different morphologies, cubic structure and agglomerated small particles (Figs. 2a-c), which coincided with previous studies that Mn_2O_3 present a cube shape, and Fe_2O_3 showed small granular shape [13–16]. Moreover, Fig. 2c exhibited the SEM image of Fe_2O_3/Mn_2O_3 composite which had already participated in five recycles. In contrast to Figs. 2a and b, there was no obvious difference in appearance which implied the composite performs excellently in stability. This was consistent with the XRD described. In addition, the mapping images were applied to display the equidistribution of elements belonging to Fe_2O_3/Mn_2O_3 composite (Figs. 2d-f). As shown, Mn, Fe and O atoms were at a coexistence distribution pattern which hinted Fe_2O_3 and Mn_2O_3 blending regularly. Finally, the EDS was used to exhibit elemental proportions of the composite (Fig. 2g), and the result was basically in line with the experimental design.

As for the degradation experiments, to evaluate activation performance of Fe_2O_3/Mn_2O_3 composite, control experiments were conducted and the outcomes were shown in Fig. 3a. As clearly shown, adsorption effect of three kinds of materials on pollutants could be neglected which indicated their limited adsorption capacity for TTZ. And the degradation rate of TTZ by pure PMS was approximately 8.8% within 30 min which meant it is difficult for separate PMS to exert its catalytic ability effectively. However, after adding the various catalysts, the removal efficiency of TTZ had increased significantly. In detail, the degradation rates raised to 66.7%, 48.8%, 97.3%, 80.2% and 89.7% when added four kinds of catalysts (Fe_2O_3/Mn_2O_3 with the mole ratio 1:1, 3:2 and 2:3, homogeneous Fe and Mn ions, respectively). It was clearly observed that with the addition of catalyst Fe_2O_3/Mn_2O_3 (mole ratio 2:3), the degradation rate of TTZ had the largest increase. That was owed to the excellent activation capacity of the catalyst for PMS, and then more active species were produced to oxidize TTZ. In addition, Fig. 3b exhibited the strength variation of unique absorbance peaks of TTZ at 427 nm. As seen, with time going on and the reaction proceeding, the peak was gradually decreased until disappeared at 30 min, which indicated TTZ was removed thoroughly by Fe_2O_3/Mn_2O_3/PMS system. Based on all of these evidences, the Fe_2O_3/Mn_2O_3 catalyst with the mole ratio of 2:3 possessed the better PMS activation performance as a result of the cooperation function of PMS and the catalyst and was used in the next series of experiments.

Besides, it is generally known that the concentration of catalyst is important for the degradation experiments in PMS system, and therefore a serious of tests were conducted to detect the influence of Fe_2O_3/Mn_2O_3 dosage with other factors fixed. In addition, the heterogeneous catalytic degradation experiment could be analyzed by the Langmuir-Hinshelwood model (Eq. 1):

$$r_0 = -\frac{dC}{dt} = k_1 k_2 C/(1 + k_2 C) \quad (1)$$

Then, as the contaminant is removed quickly, the model can be simplified as follow (Eqs. 2 and 3):

$$r_0 = -\frac{dC}{dt} \approx k_1 k_2 C \quad (2)$$

$$-\frac{dC}{C} = Kt \quad (3)$$

where r_0, k_1, k_2 and K are the total reaction rate, apparent reaction rate constant, adsorption constant and first order apparent rate constant (min^{-1}), respectively, C and t are the contaminant concentration and reaction time. In this way, we use this simplified

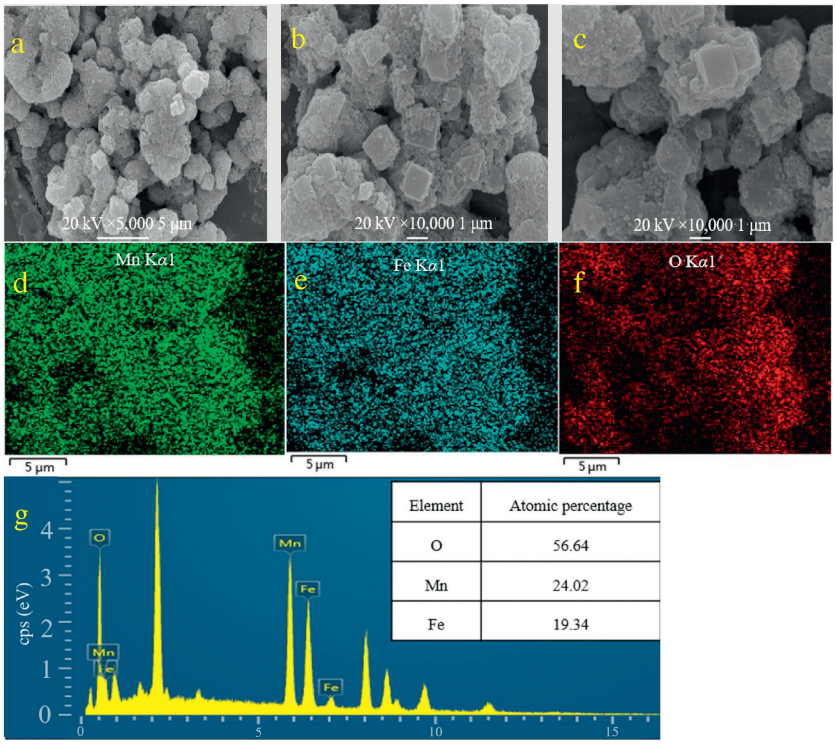

Fig. 2. Fe_2O_3/Mn_2O_3 SEM images of before (a, b) and after (c) cyclic reaction, mapping (d, e, f) and EDS (g) of Fe_2O_3/Mn_2O_3 composite.

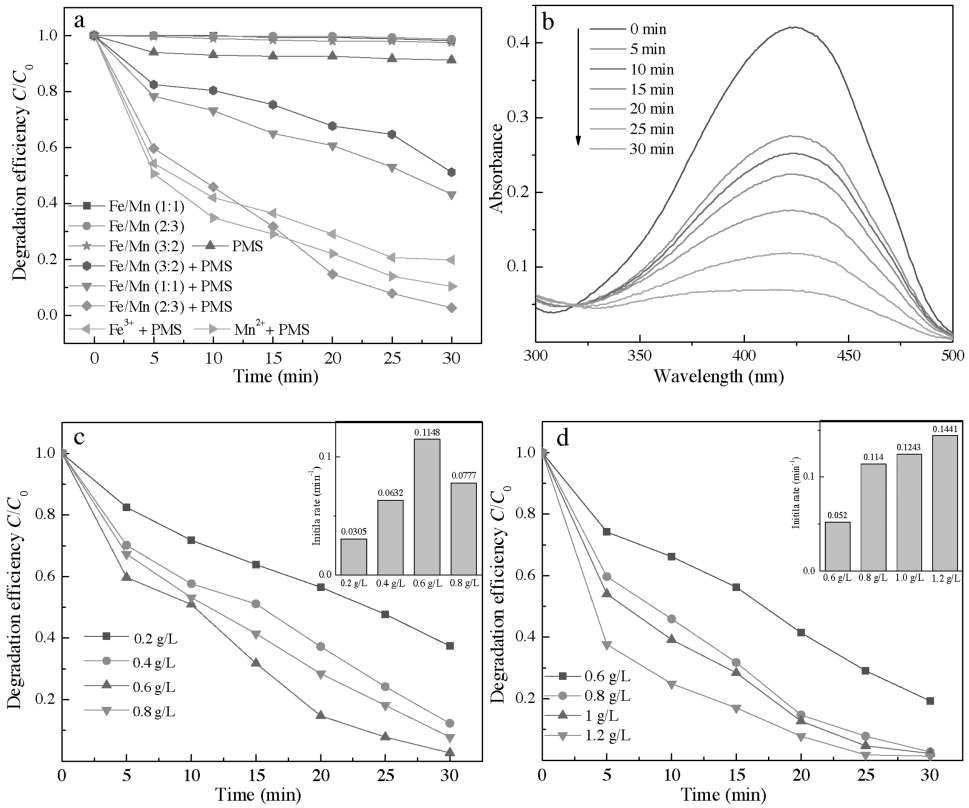

Fig. 3. Degradation of TTZ in solution under various reaction system (a), UV–vis absorption spectra of TTZ degradation (b), catalyst dosage (c), PMS concentration (d) and the insets were the corresponding initial rate (Reaction conditions: PMS concentration = 0.8 g/L, catalyst dosage = 0.6 g/L, Fe^{3+} and Mn^{2+} concentration ($FeCl_3$ and $MnCl_2$) = 0.6 g/L, TTZ concentration = 0.01 g/L, reaction temperature = 25 °C and initial pH value = 6.89 (unadjusted)).

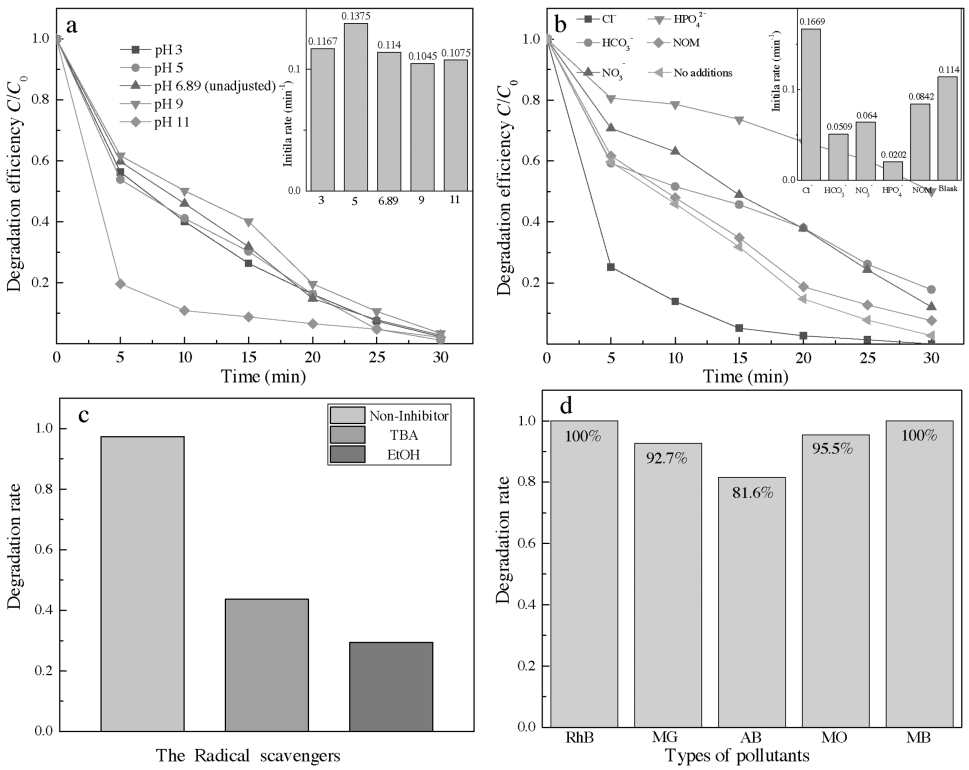

Fig. 4. Effect of different initial reaction pH (a), extra material addition (b), inhibition experiments (c) and various contaminants degradation (d) in the system of Fe_2O_3/Mn_2O_3 composite activated PMS, the inset was the corresponding initial rate (Reaction conditions: PMS concentration = 0.8 g/L, catalyst dosage = 0.6 g/L, TTZ concentration = 0.01 g/L, inhibitor dosage = 50 mmol/L, various contaminants concentration = 0.01 g/L, reaction temperature = 25 °C and initial pH 6.89 (unadjusted)).

model to fit the following degradation experiments and get the corresponding kinetic rate constant. The results were revealed in insertion of the figures. As Fig. 3c illustrated, at low catalyst dosage, the degradation rate of TTZ increased with the growth of the catalyst concentration. In detail, when the catalyst dosage raised from 0.2 g/L to 0.6 g/L, the removal efficiency increased from 62.6%–97.3% and the kinetic rate constant also raised from 0.0305 min^{-1} to 0.1148 min^{-1}. Noticeably, when the catalyst concentration raised from 0.6 g/L to 0.8 g/L, the degradation rate and kinetic rate constant were down to 92.2% and 0.0777 min^{-1}. This phenomenon could be explicated that when the catalyst dosage was increased, the active sites increased correspondingly. And to a certain extent, more active sites would generate more active species to participate in degradation process. However, when Fe_2O_3/Mn_2O_3 was excess, the reaction system had no additional PMS to active and the removal efficiency could not raise evidently. Moreover, the excess catalyst could inhibit the active species and decrease the degradation rate [21]. To sum up, in the Fe_2O_3/Mn_2O_3/PMS system, 0.6 g/L was used in the next series of experiments.

Moreover, the influence of PMS dosage on the decomposition experiments was exhibited in Fig. 3d. As shown, the degradation rate of TTZ was direct proportion to the dosage of PMS. Specifically, when the PMS concentration raised from 0.6 g/L to 1.2 g/L, the removal efficiency and kinetic rate constant growth of TTZ were from 80.7% and 0.052 min^{-1} to 98.7% and 0.1441 min^{-1}, respectively. They have both been promoted evidently. That might be because PMS is the origin of the active species, so more PMS will produce more active species and the degradation rate will grow correspondingly [22]. However, when the PMS dosage added to 1.2 g/L from 1.0 g/L, the removal efficiency and kinetic rate constant of TTZ only had a tiny change. This appearance might attribute to the fact that excessive PMS could boost the side reaction (Eqs. 4–6), and active species would reduce by the ego depletion [21–25].

$$SO_4^{\bullet-} + HSO_5^- \rightarrow SO_5^{\bullet-} + HSO_4^- \quad (4)$$

$$^{\bullet}OH + HSO_5^- \rightarrow SO_5^{\bullet-} + H_2O \quad (5)$$

$$SO_4^{\bullet-} + H_2O + HSO_5^- \rightarrow HO_2^{\bullet} + 2HSO_4^- \quad (6)$$

As a matter of fact, the pH value of the practical water is various in the different places. Therefore, it is of great significance to detect the influence of initial water pH in the degradation experiments. As exhibited in Fig. 4a, in the pH range of 3–9, the trend of removal efficiency of TTZ did not seem to change much, and the degradation rate all achieved nearly 98% within 30 min. Noticeably, when the pH raised to 11, the reaction rate speeded up remarkably. And the degradation rate attained 80% within 5 min, 93.5% within 20 min and finally reached 98% at 30 min. That demonstrated the Fe_2O_3/Mn_2O_3/PMS system had a good degradation effect in a wide range of pH. This is quite valuable in practical application. The above result could be interpreted that at the condition of higher concentration of OH^-, the inhibition reaction of H^+ to active species was weakened and then promoted the speed of TTZ decomposition (Eqs. 7 and 8) [26–28]. In addition, alkaline conditions could accelerate the following reactions of Eqs. 13, 15, 16 and 20 which also led to the raise of TTZ degradation rate.

$$H^+ + e^- + {}^{\bullet}OH \rightarrow H_2O \quad (7)$$

$$H^+ + e^- + SO_4^{\bullet-} \rightarrow HSO_4^- \quad (8)$$

In addition, in order to make the degradation experiment more suitable to the reality, some natural water substances which were abundant in natural waters were appended to the simulated sewage, such as Cl^-, HPO_4^{2-}, HCO_3^-, NO_3^- and NOM (nature organic matter). As detailedly exhibited in Fig. 4b, with the addition of HPO_4^{2-}, HCO_3^-, NO_3^- and NOM, the TTZ removal efficiency and kinetic rate constant were reduced in different degree. Moreover, the inhibitory effects were HPO_4^{2-} (50%, 0.0202 min^{-1}) > HCO_3^- (83%, 0.0509 min^{-1}) > NO_3^- (88%, 0.064 min^{-1}) > NOM (92%, 0.0842 min^{-1}) after 30 min reaction. However, the degradation experiment was accelerated after the adding of Cl^- and the degradation rate reached 100% within 30 min. The reasons of this phenomenon were listed below: (i) HPO_4^{2-} performed a strong negative effect on TTZ decomposition, which imputed the reaction of HPO_4^{2-} and active species (Eqs. 9 and 10). Both $^{\bullet}OH$ and $SO_4^{\bullet-}$ could be eliminated and the degradation rate naturally decreased [27,29,30]. (ii) HCO_3^- also could react with $^{\bullet}OH$ and $SO_4^{\bullet-}$ and generated some free radicals with low redox potential, such as $CO_3^{\bullet-}$ (E_0 = 1.78 V) and $HCO_3^{\bullet}$ (E_0 = 1.65 V) (Eq. 11). Moreover, HCO_3^- could react with PMS directly as well and produced peroxymonocarbonate (HCO_4^-, E_0 = 1.8 V). Then HCO_4^- was unstable and would decomposed into hydrogen peroxide and HCO_3^- (Eqs. 12 and 13). These factors resulted in the reduction of TTZ decomposition [29,31,32]. (iii) According to the previous researches, $NO_3^{\bullet}$ could generate by the reactions of NO_3^- with active species. And $NO_3^{\bullet}$ possessed low oxidability, thus mitigated the progress of degradation [33]. The specific reactions were shown in Eq. 14. (iv) In this research, humic acid (HA) was used to detect the influence of NOM on the TTZ degradation. HA could unite with the Fe_2O_3/Mn_2O_3, and obstruct the PMS activation process. In this way, it exhibited some inhibition effect in the Fe_2O_3/Mn_2O_3/PMS system [34]. Furthermore, after the addition of Cl^-, PMS reacted with it and produced HClO which could promote TTZ degradation (Eq. 15) [35–37].

$$HPO_4^{2-} + {}^{\bullet}OH \rightarrow OH^- + HPO_4^- \quad (9)$$

$$HPO_4^{2-} + SO_4^{\bullet-} \rightarrow SO_4^{2-} + HPO_4^- \quad (10)$$

$$HO^{\bullet} + SO_4^{\bullet-} + 2HCO_3^- \rightarrow SO_4^{2-} + HCO_3^{\bullet} + CO_3^{\bullet-} + H_2O \quad (11)$$

$$HSO_5^- + HCO_3^- \rightarrow HCO_4^- + H^+ + SO_4^{2-} \quad (12)$$

$$HCO_4^- + H_2O \rightarrow H_2O_2 + HCO_3^- \quad (13)$$

$$2NO_3^- + SO_4^{\bullet-} + HO^{\bullet} \rightarrow 2NO_3^{\bullet} + OH^- + SO_4^{2-} \quad (14)$$

$$HSO_5^- + Cl^- \rightarrow HClO + SO_4^{2-} \quad (15)$$

And then, radical inhibition experiments were conducted to detect the function of $HO^{\bullet}$ and $SO_4^{\bullet-}$ at the decomposition of TTZ. Generally speaking, ethanol (EtOH) ($SO_4^{\bullet-}$ (1.6–7.7) × 10^7 L mol^{-1} s^{-1} and $HO^{\bullet}$ (1.2–2.8) × 10^9 L mol^{-1} s^{-1}) and tertiary butanol (TBA) ($HO^{\bullet}$ (3.8–7.6) × 10^8 L mol^{-1} s^{-1}) acted as common inhibitors in the experiment [35–40]. Consequently, they were employed to radical clearance test in this work, and the results were displayed in Fig. 4c. As illustrated, with no inhibitors the degradation rate reached 97.3%, however after the mingling of TBA and EtOH it decreased to 43.7% and 29.4% within 30 min respectively. Both TBA and EtOH inhibited the TTZ degradation, in other words, both $HO^{\bullet}$ and $SO_4^{\bullet-}$ played a key role in the experiment. Moreover, in order to explore the

practicability of Fe_2O_3/Mn_2O_3/PMS system, a serious of degradation experiments for various organic pollutants were carried out, such as Rh B, MG, AB, MO and MB. Fig. 4d exhibited the degradation results, the removal efficiency were 100%, 92.7%, 81.6%, 95.5% and 100% respectively, which indicated these organic pollutants could be effectively degraded within 30 min at the Fe_2O_3/Mn_2O_3/PMS system. From the above analyses, the following conclusions could be drawn: In the Fe_2O_3/Mn_2O_3/PMS system, both $HO^•$ and $SO_4^{•-}$ were of great significance for TTZ degradation. In addition, by degrading various organic pollutants, the practicability of this system was affirmed.

Finally, for the catalyst reusability, cycle experiments were conducted for 5 times, and the outcomes were exhibited in Fig. S1a (Supporting information). Moreover, owning to the incorporation of magnetic Fe_2O_3, this catalyst was provided with certain magnetic properties. Fig. S1b (Supporting information) exhibited the magnetism of catalyst, and Fe_2O_3/Mn_2O_3 were drawn to an external magnet without difficulty within 1 min, which were significant to the recycling. As seen, the degradation rate of TTZ within 30 min stabled at about 95% basically in this five cyclic experiments. Meanwhile, the ions leaching of Fe_2O_3/Mn_2O_3 were also measured and the ion concentration released from Fe_2O_3 and Mn_2O_3 were 0.136 mg/L and 0.006 mg/L which were 0.02% of the total catalyst. Therefore, based on these results and the XRD atlases, the Fe_2O_3/Mn_2O_3 catalyst possessed excellent stability and was more environmentally friendly and it is a promising catalyst.

According to the debate above and previous researches, the potential mechanism of the Fe_2O_3/Mn_2O_3/PMS system for TTZ degradation was proposed. Firstly, pure PMS reacted with TTZ directly without the participation of active species (Eqs. 16). And then, Mn(III) and Fe(III) on Fe_2O_3/Mn_2O_3 surface activated PMS to produce $SO_4^{•-}$ and $SO_5^{•-}$ respectively (Eqs. 17 and 18). Because of this, part of the Mn(III) and Fe(III) transformed to Mn(IV) and Fe(II), which was consistent with the XPS atlases result [19]. Meanwhile, the generated Mn(IV) and Fe(II) were able to re-form Mn(III) and Fe(III) by reacting with HSO_5^- (Eqs. 19–21). In addition, because the oxidability of Mn(IV) is stronger than Fe (III), the Eq. (22) could take place to regenerate Fe(III) and meanwhile Mn(IV)/Mn(III) redox pairs become the main role that responsible for PMS activation. It was precisely for this reason that the TTZ degradation experiments could carry on and active species could generate continuously. In addition, the $SO_5^{•-}$ could break down into $SO_4^{•-}$ and O_2 in aqueous solution (Eq. 23). $SO_4^{•-}$ was able to react with H_2O as well to generate $HO^•$ (Eq. 24) [41–47]. Finally, all of the $HO^•$ and $SO_4^{•-}$ completely oxidized and decomposed TTZ (Eq. 25) and the thorough oxidation reactions were displayed below:

$$TTZ + HSO_5^- + 2e^- \rightarrow SO_4^{2-} + OH^- + \text{products} \quad (16)$$

$$Mn^{3+} + HSO_5^- \rightarrow Mn^{4+} + SO_4^{•-} + OH^- \quad (17)$$

$$HSO_5^- + Fe^{3+} \rightarrow SO_5^{•-} + Fe^{2+} + H^+ \quad (18)$$

$$Mn^{4+} + HSO_5^- \rightarrow Mn^{3+} + SO_5^{•-} + H^+ \quad (19)$$

$$HSO_5^- + Fe^{2+} \rightarrow OH^- + Fe^{3+} + SO_4^{•-} \quad (20)$$

$$HSO_5^- + Fe^{2+} \rightarrow Fe^{3+} + SO_4^{2-} + HO^• \quad (21)$$

$$Mn^{4+} + Fe^{2+} \rightarrow Mn^{3+} + Fe^{3+} \quad (22)$$

$$2SO_5^{•-} \rightarrow 2SO_4^{•-} + O_2 \quad (23)$$

$$SO_4^{•-} + H_2O \rightarrow HO^• + SO_4^{2-} + H^+ \quad (24)$$

$$TTZ + SO_4^{•-}/HO^• \rightarrow \text{products} + SO_4^{2-} + H_2O \quad (25)$$

In summary, the Fe_2O_3/Mn_2O_3 catalyst was synthesized by simple two-step method in this work, and several methods (XRD, SEM, EDS, Mapping and XPS) were conducted to characterize it. And then, TTZ decomposition experiments were carried out under various conditions in the Fe_2O_3/Mn_2O_3/PMS system to detect the activation properties of catalysts. The discussion results showed that (i) through a series of characterization experiments, the Fe_2O_3/Mn_2O_3 catalyst was proved to be successfully prepared. (ii) Different degradation experiments confirmed the great PMS activation capacity of Fe_2O_3/Mn_2O_3 (Fe/Mn = 2:3), the removal efficiency of TTZ (10 mg/L) reached 97.3% within 30 min under the Fe_2O_3/Mn_2O_3/PMS system. The optimum reaction conditions were also found, such as catalyst dosage (0.6 g/L), PMS concentration (0.8 g/L) and the initial pH 11. In addition, inhibitor experiments indicated both the $HO^•$ and $SO_4^{•-}$ played a vital role in the experiments. And HPO_4^{2-}, HCO_3^-, NO_3^- and NOM could slow down the experiments progressing while Cl^- could boost it. (iii) Reusability and ions leaching experiments as well as the used catalyst XRD and SEM images implied the excellent stability and cyclicity of the Fe_2O_3/Mn_2O_3 composite. (iv) Based on the XPS and the experiments results, the possible mechanism of TTZ degradation was proposed.

Declaration of competing interest

We have no conflicts of interest to declare.

Acknowledgments

This work was kindly funded by the National Natural Science Foundation of China (No. 51978319), National College Student Innovation and Entrepreneurship Training Program of Lanzhou University and Key Laboratory of Comprehensive and Highly Efficient Utilization of Salt Lake Resources, Qinghai Institute of Salt Lake, Chinese Academy of Sciences.

Appendix A. Supplementary data

Supplementary material related to this article can be found, in the online version, at doi:https://doi.org/10.1016/j.cclet.2020.02.033.

References

[1] Y. Wang, Y. Mu, J. Hu, Q. Zhuang, Y. Ni, Spectrochim. Acta A: Mol. Biomol. Spectrosc. 214 (2019) 445–450.
[2] S. Sahnoun, M. Boutahala, Int. J. Biol. Macromol. 114 (2018) 1345–1353.
[3] S. Balu, S. Velmurugan, S. Palanisamy, S.W. Chen, J. Taiwan Inst, Chem. E 99 (2019) 258–267.
[4] C. Zhang, G. Ren, W. Wang, et al., Sep. Purif. Technol. 208 (2019) 76–82.
[5] H. Ouassif, E.M. Moujahid, R. Lahkale, et al., Surf. Interface Anal. 18 (2020) 100401.
[6] M. Marković, S. Marinović, T. Mudrinić, et al., Appl. Clay Sci. 182 (2019) 105276.
[7] Z. Wang, X. Zhang, H. Zhang, et al., Sep. Purif. Technol. 215 (2019) 528–539.
[8] R. Guo, Q. Meng, H. Zhang, et al., Chem. Eng. J. 355 (2019) 952–962.
[9] Q. Ma, H. Zhang, X. Zhang, et al., Chem. Eng. J. 360 (2019) 848–860.
[10] H. Zhang, J. Wang, X. Zhang, B. Li, X. Cheng, Chem. Eng. J. 369 (2019) 834–844.
[11] N. Tian, X. Tian, Y. Nie, et al., Chem. Eng. J. 355 (2019) 448–456.
[12] J. Huang, Y. Dai, K. Singewald, et al., Chem. Eng. J. 370 (2019) 906–915.
[13] R. Khaghani, B. Kakavandi, K. Ghadirinejad, E. Dehghani Fard, A. Asadi, Microporous Mesoporous Mater. 284 (2019) 111–121.
[14] Q. Ma, X. Zhang, R. Guo, et al., Sep. Purif. Technol. 210 (2019) 335–342.

[15] J. Zhao, J. Nan, Z. Zhao, N. Li, Catal. Commun. 102 (2017) 5–8.
[16] N. Parveen, Z. Khan, S.A. Ansari, et al., Chem. Eng. J. 360 (2019) 415–422.
[17] M. Nasiri, P. Sangpour, S. Yousefzadeh, M. Bagheri, J. Environ, Chem. Eng. 7 (2019)102999.
[18] D. Wang, L. Jin, Y. Li, et al., Fuel Process. Technol. 191 (2019) 20–28.
[19] Q. Yang, X. Yang, Y. Yan, et al., Chem. Eng. J. 348 (2018) 263–270.
[20] J. Deng, S. Feng, X. Ma, et al., Sep. Purif. Technol. 167 (2016) 181–189.
[21] G. Chen, L.C. Nengzi, B. Li, et al., Sci. Total Environ. 695 (2019) 133963.
[22] G. Chen, X. Zhang, Y. Gao, et al., Sep. Purif. Technol. 213 (2019) 456–464.
[23] J. Li, Y. Wan, Y. Li, G. Yao, B. Lai, Appl. Catal. B: Environ. 256 (2019) 117782.
[24] J. Yan, J. Li, J. Peng, et al., Chem. Eng. J. 359 (2019) 1097–1110.
[25] Z. Wang, L.C. Nengzi, X. Zhang, Z. Zhao, X. Cheng, Chem. Eng. J. 381 (2020) 122517.
[26] F. Ghanbari, M. Ahmadi, F. Gohari, Sep. Purif. Technol. 228 (2019) 115732.
[27] F. Ghanbari, C.A. Martínez-Huitle, J. Electroana. Chem. 847 (2019) 113182.
[28] M. Ahmadi, F. Ghanbari, Environ. Sci. Pollut. Res. Int. 25 (2018) 6003–6014.
[29] Y.H. Huang, Y.F. Huang, C.I. Huang, C.Y. Chen, J. Hazard. Mater. 170 (2009) 1110–1118.
[30] N. Jaafarzadeh, F. Ghanbari, M. Moradi, Korean J. Chem. Eng. 32 (2015) 458–464.
[31] M. Ahmadi, F. Ghanbari, Mater. Res. Bull. 111 (2019) 43–52.
[32] J. Li, M. Xu, G. Yao, B. Lai, Chem. Eng. J. 348 (2018) 1012–1024.
[33] M. Nie, Y. Deng, S. Nie, et al., Chem. Eng. J. 369 (2019) 35–45.
[34] X. Xu, D. Tang, J. Cai, et al., Appl. Catal. B: Environ. 251 (2019) 273–282.
[35] C. Li, Y. Huang, X. Dong, et al., Appl. Catal. B: Environ. 247 (2019) 10–23.
[36] P. Duan, T. Ma, Y. Yue, et al., Environ. Sci. Nano 6 (2019) 1799–1811.
[37] M. Ahmadi, F. Ghanbari, A. Alvarez, S. Silva Martinez, Korean J. Chem. Eng. 34 (2017) 2154–2161.
[38] S. Wang, J. Wang, Chem. Eng. J. 379 (2020) 122361.
[39] R. Xie, J. Ji, K. Guo, et al., Chem. Eng. J. 356 (2019) 632–640.
[40] Y. Huang, X. Zhang, G. Zhu, et al., Sep. Purif. Technol. 215 (2019) 490–499.
[41] Y. Shang, C. Chen, P. Zhang, et al., Chem. Eng. J. 375 (2019) 122004.
[42] C. Chen, T. Ma, Y. Shang, et al., Appl. Catal. B: Environ. 250 (2019) 382–395.
[43] C. Gong, F. Chen, Q. Yang, et al., Chem. Eng. J. 321 (2017) 222–232.
[44] H. Lu, M. Sui, B. Yuan, J. Wang, Y. Lv, Chem. Eng. J. 357 (2019) 140–149.
[45] J. Deng, Y. Ge, C. Tan, et al., Chem. Eng. J. 330 (2017) 1390–1400.
[46] C. Huang, Y. Wang, et al., Sep. Purif. Technol. 230 (2020) 115877.
[47] E. Saputra, H. Zhang, Q. Liu, H. Sun, S. Wang, Chemosphere 159 (2016) 351–358.